Published in final edited form as:
J Comp Neurol. 2010 August 15; 518(16): 3254–3271. doi:10.1002/cne.22398.

Unmyelinated Auditory Type I Spiral Ganglion Neurons in Congenic Ly5.1 Mice

Vinu Jyothi[1], **Manna Li**[1], **Lauren A. Kilpatrick**[2], **Smythe Nancy**[2], **Amanda C. LaRue**[1], **Daohong Zhou**[1], **Bradley A. Schulte**[1,2], **Richard A. Schmiedt**[2], and **Hainan Lang**[*,1]

[1]Department of Pathology and Laboratory Medicine, Medical University of South Carolina, Charleston, SC 29425, United States

[2]Department of Otolaryngology – Head & Neck Surgery, Medical University of South Carolina, Charleston, SC 29425, United States

Abstract

With the exception of humans, the somata of type I spiral ganglion neurons (SGNs) of most mammalian species are heavily myelinated. In an earlier study, we used Ly5.1 congenic mice as transplant recipients to investigate the role of hematopoietic stem cells in the adult mouse inner ear. An unanticipated finding was that a large percentage of the SGNs in this strain were unmyelinated. Further characterization of the auditory phenotype of young adult Ly5.1 mice in the present study revealed several unusual characteristics including: 1) large aggregates of unmyelinated SGNs in the apical and middle turns; 2) symmetrical junction-like contacts between the unmyelinated neurons; 3) abnormal expression patterns for CNPase and connexin 29 in the SGN clusters; 4) reduced SGN density in the basal cochlea without a corresponding loss of sensory hair cells; 5) significantly delayed auditory brainstem response (ABR) wave I latencies at low and middle frequencies as compared to control mice with similar ABR threshold and 6) elevated ABR thresholds and deceased wave I amplitudes at high frequencies. Taken together, these data suggest a defect in Schwann cells that leads to incomplete myelinization of SGNs during cochlear development. The Ly5.1 mouse strain appears to be the only rodent model so far identified with a high degree of the “human-like” feature of unmyelinated SGNs that aggregate into neural clusters. Thus, this strain may provide a suitable animal platform for modeling human auditory information processing such as synchronous neural activity and other auditory response properties.

Keywords

primary auditory nerve; myelinization; neural aggregation; inner ear; hearing loss; auditory brainstem response

INTRODUCTION

Hematopoietic stem cell transplantation is an essential medical procedure used extensively in the treatment of neoplastic diseases. The mouse is an important animal model for preclinical studies of bone marrow transplantation. The B6.SJL-*Ptprc*^{a} *Pepc*^{b}/BoyJ mouse, also termed Ly5.1, is a congenic strain widely used as a recipient in bone marrow transplant studies because it carries a differential Ly5 allelic form (Saga et al., 1987). Ly5, also

Corresponding author: Hainan Lang, Department of Pathology and Laboratory Medicine, Medical University of South Carolina, 165 Ashley Avenue, PO BOX 250908, Charleston, SC 29425, USA, Tel: 843-792-2711, Fax: 843-792-0368, langh@musc.edu.

referred to as protein tyrosine phosphatase receptor C (*Ptprc*) or CD 45, is a well known leukocyte common antigen used for the identification of hematopoietic stem cells (Zebedee et al., 1991). The Ly5 gene exists in multiple forms including allelic forms Ly5.1 and Ly5.2. This distinction permits the identification and differentiation of the donor cells (those from Ly5.2 mice) from recipient cells (those from Ly5.1 mice) using immunofluorescent staining and flow cytometry.

Spiral ganglion neurons (SGNs) are the primary carriers of auditory information from sensory hair cells to the brain. There are two populations of SGNs in mammalian ears, type I and type II neurons (Spoendlin 1969; Kiang et al., 1982; Romand and Romand 1990). Recent studies have demonstrated that the type I and type II neurons have their own electrophysiological characteristics, and these differentiated features suggest that these two populations of SGNs may play different roles in auditory information processing (Jagger and Housley 2003; Reid et al., 2004; Weisz et al., 2009).

Myelin is an electrically insulating material that forms the myelin sheath around some neuronal processes and cell bodies. It essential for the proper functioning of the nervous system, e.g., enhancing the speed of the neural transmission (Hildebrand, 1993). In the mammalian inner ear, myelination is preceded by the ensheathment of the neuronal cell body by two or three layers of Schwann cell cytoplasmic processes. With the exception of humans, type I SGNs in most mammalian species including rodents are heavily myelinated. The peripheral processes of type I neurons, which represent approximately 90–95% of SGNs, synapse with inner hair cells. The remaining neurons are unmyelinated type II neurons. Type II neurons are located primarily in the periphery of the spiral ganglion and innervate outer hair cells. In a previous study, we used congenic Ly5.1 mice as transplant recipients to study the role of hematopoietic stem cells in the adult mouse inner ear (Lang et al., 2006a). Surprisingly, morphological evaluation of Ly5.1 mouse cochleas revealed that the majority of SGNs in the apical and middle turns were unmyelinated and often aggregated into neuronal clusters. Similarities between these neuronal aggregates and the unmyelinated SGNs in humans led us to further investigate their structural and functional characteristics.

Ly5.1 mice carry the *Ptprc*^{a} allele and closed lined *Pepc*^{b}allele. *Ptprc* is a family of protein-tyrosine phosphatase genes involved in the regulation of cell growth and differentiation. The current use of the *Ptprc* designation for Ly5 was based on human placental protein-tyrosine phosphatase 1B which is homologous to the Ly5 (or CD 45) protein (Charbonneau et al., 1988). Previous studies have demonstrated that receptor protein tyrosine phosphatases play an important role in neuronal morphogenesis in a variety of different vertebrate and non-vertebrate systems (Johnson and Vactor 2003; Dunah et al., 2005; Stepanek et al., 2005). It is possible that the alteration of protein-tyrosine phosphatase-related genes has played a role in producing the unusual phenotype of auditory neurons in Ly5.1 mice. Since the Ly5.1 mice were created on a C57BL/6J and SJL/J background, these two strains were used as controls in this study. It is well known that C57BL/6J mice develop progressive, high-frequency hearing loss by middle age with associated pathological changes including the degeneration of sensory hair cells, SGNs and fibrocytes in the spiral ligament (Mikaelian et al., 1974; Cohen et al., 1990; Hequembourg and Liberman 2001). Previous studies of the SJL/J strain have revealed a significant loss in vestibular function with no associated hearing loss, but comprehensive histopathological analyses are lacking in these studies (Jones et al., 2006; Zhou et al., 2006). CBA/CaJ mice were used as a third control strain in this study. This strain develops hearing loss at a very late age and has been widely used as the “standard normal control” strain in previous studies (Zheng et al., 1999).

MATERIALS AND METHODS

Animals

Ly5.1 (B6.SJL-*Ptprc*^{a} *Pepc*^{b}/BoyJ), C57BL/6J, SJL/J, and CBA/CaJ mice were purchased from The Jackson Laboratory (Bar Harbor, ME, see database for Ly5.1 mice at http://jaxmice.jax.org/strain/002014.html, Stock# 002014; C57BL/6J at http://jaxmice.jax.org/strain/000664.html, Stock# 000664;; SJL/J mice at http://jaxmice.jax.org/strain/000686.html, Stock# 000686; CBA/CaJ mice at http://jaxmice.jax.org/strain/000654.html, Stock# 000654). Ly5.1 strain was created by serially backcrossing SJL/J mice which carry the *Ptprc*^{a} allele with C57BL/6J mice which carry the *Ptprc*^{b} allele and selecting for the *Ptprc*^{a} allele by genotyping (Shen et al., 1985). The Jackson Laboratory obtained the Ly5.1 strain from Edward Boys at Sloan Kettering at generation N22 in 1990. SJL strain was developed at the Jackson Laboratory in 1955 from three different sources of Swiss Webster mice. The CBA/CaJ strain was initially bred for longevity and a low incidence of spontaneous mammary tumors. All the mice used in this study were generated by breeding homozygotes from original breeding pairs for only 2–3 generations. All mice were kept in a low-noise environment at the Animal Research Facility of the Medical University of South Carolina. All mice received food and water ad libitum and were maintained on a 12-hour light/dark cycle. Mice of both genders aged 1 to 1.5 and 8 months were used in the study. Inner ear tissues also were harvested from postnatal P0 Ly5.1 and CBA/CaJ mice. P0 was defined as the day of birth. Note that the results showed no significant difference in morphological and physiological characteristics between mice aged 1 month and those aged 1.5 months. Throughout the paper, the term “young adult mice” applies to all these 1–1.5 month-old mice if no other statement has been included. All aspects of the animal research were conducted in accordance with the guidelines of the Institutional Animal Care and Use Committee of the Medical University of South Carolina. Prior to data acquisition, mice were examined for signs of external ear canal and middle ear obstruction. Mice with any symptoms of ear infection were excluded from the study.

Physiological procedures

Mice were anesthetized by an intraperitoneal injection of xylazine (20mg/kg) and ketamine (100mg/kg) and placed in a head restraint device in a sound-isolation room. CBA/CaJ (n=26), Ly5.1 (n=21), C57BL/6J (n=20) and SJL/J (n=8) aged 1 to 1.5 month-old young adult mice were used for physiological measurements. Auditory brainstem responses (ABRs) were recorded via customized needle electrodes inserted at the vertex (+) and test-side mastoid (−), with a ground in the control-side leg. The acoustic stimuli were generated using Tucker Davis Technologies equipment III (Tucker-Davis Technologies, Gainsville, FL, USA) and a SigGen software package. The calibration was completed using a Knowles microphone in a probe tube clipped to the pinna. The signals were delivered into the mouse ear canal through a 10 mm long (3–5 mm diameter) plastic tube. ABR thresholds, defined as the lowest sound levels at which the response peaks are clearly present as read by the eye from stacked wave forms, were obtained. ABRs were evoked at half octave frequencies from 4 to 45 kHz with 5 ms duration tone pips with $\cos^2$ rise/fall times of 0.5 ms delivered at 31/s. Sound levels were reduced in 5-dB steps from 90 dB SPL to 10 dB SPL below thresholds. For ABR amplitudes and latencies vs. level functions (I/O function), the wave I peaks were identified by visual inspection at each sound level with the peak-to-peak wave I amplitude and latency computed. At each sound level, 300–500 responses were averaged, using an “artifact reject” whereby response waves were discarded when peak to peak amplitude exceeded 50 mV. Physiological results of each mouse strain were analyzed for individual frequencies, and then averaged for each of these frequencies from 4.0 to 40 kHz.

Morphological and immunohistochemical analysis

CBA/CaJ (n=26), Ly5.1 (n= 16), C57BL/6J (n=15) and SJL/J (n=8) young adult mice aged 1–1.5 months were used for the following procedures including morphological and immunohistochemical analysis. In addition, newborn (P0) (n=3 per group) and 8 month-old (n=5 per group) CBA/CaJ and Ly5.1 mice were used for morphological observations. Morphological findings from these newborn and middle-aged mice are provided in Supplementary Figures 1 and 2. For morphological observation, the anesthetized animals were perfused via cardiac catheter first with 10 ml of normal saline containing 0.1 % sodium nitrite and then 15 ml of a mixture of 4% paraformaldehyde and 2% glutaraldehyde in 0.1M phosphate buffer, pH 7.4. After removing the stapes and opening the oval and round windows, 0.5 ml of fixative was perfused gently into the scala vestibuli through the oval window. The inner ears were dissected free and immersed in fixative overnight at 4 °C. Decalcification was completed by immersion in 100 ml of 120 mM solution of ethylenediamine tetracetic acid (EDTA), pH 7.2, with gentle stirring at room temperature for 2–3 days with daily changes of the EDTA solution. The tissues were postfixed with a 1% osmium tetroxide for 1 hour in the dark, dehydrated and embedded in Epon LX 112 resin. Semi-thin sections approximately 1 μm thick were cut and stained with toluidine blue. Micrographs were taken at 100x magnification on a Zeiss Axio Observer D1 with a digital AxioCam camera. Individual images were opened in Adobe Photoshop CS2, then copied and pasted into a new canvas with sufficient size to reconstruct the cochlea. At high screen magnification, each individual layer was adjusted to a more precise location and locked together using the Photomerge feature of Adobe Photoshop CS2 software.

Quantitative analysis of non-myelinated neurons and neural cell loss was performed using cochleas from four to six young adult mice of each strain. Cell count data were collected from 5–10 1μm mid-modiolar sections per cochlea. The sections used for counting were at least 15 μm apart (e.g., cell counting was performed on 1 in every 16 serial sections). Because simple profile-based counts can result in a substantial over-counting bias (Guillery 2002), the Abercromie correction factors were applied. The correction factor was determined by dividing the section thickness (1 μm) by the sum of the section thickness and the average diameter (height) of the neuronal nucleus: T/T+H, where T= section thickness and H=average nuclear height. The average nuclear diameter was determined separately for each mouse strain by measuring the diameter of 20 nuclei in midmodiolar sections of Rosenthal's canal randomly selected from the basal, middle and apical turns. The calculated correction factors in apical, middle and basal turns were 0.114, 0.108 and 0.115 for CBA/CaJ mice, 0.112, 0.108 and 0.107 for Ly5.1 mice, 0.109, 0.112 and 0.118 for C57BL/6J and 0.108, 0.107 and 0.109 for SJL/J mice. The average cell counts were multiplied by the appropriate correction factor to determine the percentage of the non-myelinated neurons and neural cell loss in each mouse strain.

For immunohistochemistry, the inner ears were prepared following the procedure described above but substituting 4 % paraformaldehyde as fixative, decalcified with EDTA, cryprotected in 30 % sucrose in PBS and embedded in Tissue-Tek OCT compound (Electron Microscopy Science, FT. Washington, PA). Frozen sections were cut at 15 μm thickness and stained using immunofluorescence methods modified slightly from those previously described (Lang et al., 2008). Briefly, sections were immersed in blocking solution for 30 min and then incubated overnight at 4 °C with a primary antibody diluted in PBS. The primary antibodies used in this study were mouse anti-CNPase (1:150, 6.7 μg/ml, MAB326; Chemicon, Temecula, CA), rabbit anti-class III β-tubulin (TuJ1, 1:200, 5 μg/ml, MRB-435p; Covance, Emeryville, CA), mouse anti-neurofilament 200 (1:200, 16 μg/ml, Clone N52, N0142; Sigma, Atlanta, GA), rabbit anti-Na, K-ATPase (1:2000, 6 μg/ml, 31b, Dr. George Siegel, University of Michigan Medical School, Ann Arbor, MI), rabbit anti-connexin 29 (1:200, 1 μg/ml, sc-68377; Santa Cruz Biotechnology, Santa Cruz, CA), rabbit anti-myosin-

VIIa (1:150, 2.5 μg/ml, 25–6790; Proteus Biosciences, Ramona, CA), mouse anti-peripherin (1:150, 1 μg/ml, AB1530; Chemcon, Temecula, CA) and rabbit anti-peripherin (1:200, 10 μg/ml, AB1527; Chemicon, Temecula, CA) (See Table 1).

CNPase is a myelin-specific enzyme expressed by oligodendrocytes in the central nervous system and Schwann cells in the peripheral nervous system (Sprinkle 1989). The mouse monoclonal antibody to CNPase was raised against human brain 2', 3'-cyclic nucleotide 3'-phosphodiesterase. It reacts with the 46 and 48 kD polypepetides in SDS-PAGE blots of human brain tissue extracts and is widely used as a marker to label Schwann cells and myelin sheaths (manufacturer's technical information). The expression of CNPase in Schwann cells and myelin sheaths were previously reported in adult mouse SGNs (Kim et al., 1984).

The mouse monoclonal antibody to neurofilament 200 (phosphorylated and non-phosphorylated, clone N52) was prepared against the carboxyterminal tail segment of enzymatically dephosphorylated pig neurofilament H-subunit. The antibody reacts with the neurofilament of molecular weight 200kD in rat spinal cord extracts (manufacturer's technical information). When tested by immunoblotting on pig neurofilament polypeptides, the antibody reacts with an epitope in the tail domain of neurofilament 200, which is present on both the phosphorylated and non-phosphorylated forms of this polypeptide (manufacturer's technical information). This antibody has been extensively used to label SGNs in adult mouse inner ear (Wise et al., 2005; Lang et al., 2006b; 2008).

The neuronal class III β-tubulin (TUJ1) rabbit monoclonal antibody was raised against microtubules derived from rat brain and reacts with an epitope located in the extreme carboxy terminus of class III β-tubulin (Lee et al., 1990). TUJ1 is highly selective for neuron-specific class III β-tubulin, but not to glial β-tubulin (manufacturer's technical information). The TUJ1 antibody specifically recognizes the ~59 kDa class III β-tubulin band on Western blots of rat and chicken brain (Lee et al., 1990). A previous study demonstrated that TuJ1 was highly expressed in type I SGNs of mouse inner ear (Sekerkova et al., 2008).

The rabbit polyclonal antiserum to Na, K-ATPase (31b), kindly provided by Dr. George Siegel, University of Michigan Medical School (Ann Arbor, MI), was raised against the catalytic subunit from bovine brain cortex Na, K-ATPase and recognizes the α1, α2 and α3 isoforms of catalytic subunit as determined by Western Blots from mouse and bovine brain tissues (Heiber et al., 1989) and comparative immunohistochemistry in gerbil and mouse cochlear tissues (Schulte and Adams 1989; McGuirt and Schulte 1994).

The rabbit polyclonal anti-connexin 29 antiserum was prepared against a peptide containing amino acids 171–258 mapping at the C-terminus of mouse connexin 29. The antiserum stained a single band of 31 kDa molecular weight on Western blots (manufacturer's technical information). Staining on the sections of adult mouse inner ears produced a pattern of connexin 29 immunoreactivity in auditory nerve that was identical to previous results (Tang et al., 2006).

Peripherin is a 56–58 kDa class III intermediate filament protein expressed extensively in the peripheral nervous system. Both the mouse monoclonal and the rabbit polyclonal anti-peripherin antibodies were raised against the electrophoretically pure trp-E-peripherin fusion protein purified from bacterial inclusion bodies, containing all but the 4 N-terminal amino acids of rat peripherin (Gorham et al., 1990; manufacturer's technical information). Rabbit anti-peripherin reacts cleanly with a 57 kD band from rat brain homogenates and does not recognize vimentin, GFAP, α internexin or any of the neurofilament subunits

(manufacturer's technical information). Both antibodies are used as markers for type II SGNs in the rodent inner ear (Hafidi, 1998; Reid et a., 2004; Lang et al., 2005).

Myosin VIIA is one of the unconventional members of the myosin molecular motor superfamily that move along filamentous actin. Evidences from immunofluorescence studies have shown that myosin VIIA is highly expressed by sensory hair cells in the mammalian inner ear (Avraham et al., 1995; Gubbels et al., 2008). The rabbit polyclonal anti-myosin VIIA was raised against a peptide consisting of amino acids 880–1077 from the tail region of human myosin-VIIA (manufacturer's technical information). This antibody recognizes myosin VIIA of human, mouse, rat, pig, avian and amphibian origin (manufacturer's technical information).

For double staining protocols, the primary antibodies selected were generated in different species (e.g., one mouse monoclonal antibody with one rabbit or goat polyclonal antibody). Secondary antibodies were biotinylated and binding was detected with FITC-conjugated avidin D (1:150) (Vector, Burlingame, CA). The procedure for detection of the secondary antigen was the same as for the first antigen but substituting Texas-red conjugated avidin D (1:150) (Vector, Burlingame, CA) for visualization. Nuclei were counterstained with bisbenzimide. Control staining for all primary antibodies included omission or substitution of the primary antibody with similar dilutions of non-immune serum of the appropriate species. No specific staining was detected in any of these control experiments.

The sections were examined either with a Zeiss Axio Observer or a Zeiss LSM5 Pascal confocal microscope (Carl Zeiss Inc., Jena, Germany). The captured images were processed using Image Pro Plus software (Media Cybernetics, MD) and Zeiss LSM Image Browser Version 3,2,0,70 (Carl Zeiss Inc., Jena, Germany). Adobe Photoshop CS2 was employed to adjust brightness, contrast, and sharpness of images with identical setting for all panels. Alterations were not performed on images used for quantitative purposes.

Preparation of cytocochleograms

The procedure for counting hair cells on surface preparations of the organ of Corti was described previously (Lang et al., 2006b). Five young adult mice of each strain were used for hair cell counting. The basilar membrane was carefully dissected from the fixed cochlea, stained for 20 min with FITC-labeled phalloidin (1 μg/ml in PBS) to label filamentous actin and stained for 10 min with PI (1 μg/ml in PBS) to label the nuclei. The structural integrity of sensory hair cells was identified by the presence of the actin-rich hair cell bundles, the actin belt that rings the surface of the cell and a normal-looking nucleus. Hair cells within each 200 μm-long segment along the length of the basilar membrane were counted under a Zeiss Axio Observer. Hair cell loss in Ly5.1 and C57BL/6J mice was expressed as a percentage of the "standard normal" number of hair cells in the CBA/CaJ mouse as previously reported (Ding et al., 2001) and plotted versus distance from the apex and cochlear frequency. Cochlear locations were translated into cochlear frequencies using a map based on that of Ehret (1983).

Data analysis

Unless otherwise specified, all data in the figures are presented as mean ± standard error of the mean (SEM). Data for the percentage of unmyelinated SGNs, the density of SGNs, ABR thresholds, ABR wave I amplitude and latency functions were analyzed by one- and two-way ANOVA or two tailed, unpaired *t* test (SPSS, Chicago, IL). A value of $p < 0.01$ was considered to be statistically significant.

RESULTS

Unmyelinated SGNs and neural aggregation in the apical and middle turns

A mid-modiolar section from the apical turn of a CBA/CaJ young adult mouse illustrated what is considered to be typical SGN morphology in most mammalian ears (Fig. 1A). The majority of neurons can be classified as type I neurons based on their size, location and nuclear and cytoplasmic staining patterns. The perikaryon of each type I neuron was surrounded by a dark blue line, which represents the myelin sheath. Most type I neurons were separated from their neighboring neurons by nerve fibers. A few type II neurons were present in the lateral portion of the spiral ganglion close to the root of the osseous spiral lamina.

In Ly5.1 young adult mice, a large number of SGNs in the apical and middle turns of the cochlea lacked myelin sheaths around their cell bodies (Figs. 1B, E). These unsheathed neurons aggregated into various sized clusters. Cell counts on over 600 semi-thin sections randomly taken from 12 ears revealed that the number of neurons in each cluster ranged from 4 to 30 with an average of 16 ± 7.5. In contrast to the apical and middle turns, the majority of SGNs in the basal turn of Ly5.1 mice were myelinated (Figs. 1F, 3A). No discernable abnormalities were observed in nerve processes in the apical and middle turns of these mice (Figs. 1B, E).

Neuronal clusters were also seen in the apical turn of C57BL/6J mice (Fig. 1C), an observation consistent with previous studies in young and old adult C57BL/6J mice (Cohen et al., 1990;Hequembourg and Liberman 2001;Ohlemiller and Gagnon 2004). However, these clusters were much less frequent and significantly smaller than those in Ly5.1 mice. Cell counts on 50 semi-thin sections randomly selected from five adult C57BL/6J mice revealed a range of 3 to 11 neurons per cluster with an average of 6 ± 2.73 neurons. The percentage of unmyelinated neurons in the apical turn of C57BL/6J mice also was significantly less than that of Ly5.1 mice (Fig. 1F).

Neural clusters were extremely rare in CBA/CaJ and SJL/J young adult mice. Examination of over 600 sections from 12 CBA/CaJ mice revealed only one neuronal cluster in an apical turn (data not shown). No neuronal aggregation was seen in over 200 sections randomly taken from five SJL/J mice. The morphology of type I and II SGNs in the apical turn in SJL/J mice (Fig. 1D) was similar to that of CBA/CaJ mice.

Results of cell counts of unmyelinated SGNs in the apical, middle and basal turns of the four mouse strains were illustrated in Fig. 1F. The percentage of unmyelinated neurons in the apical turn is 81.6 % for Ly5.1, 21.5% for C57BL/6J, 9.3% for CBA/CaJ and 9.8% for SJL/J mice. In the middle turn, 43% of neurons were unmyelinated in Ly5.1 mice, compared with 4.9%, 6.2% and 9% for C57BL/6J, CBA/CaJ and SJL/J mice, respectively. The percentage of unmyelinated SGNs in the apical and middle turns of Ly5.1 mice was significantly higher than that of the other three strains ($p<0.01$). In contrast, the percentage of unmyelinated neurons in the basal turns of the four strains ranged from 5.3 to 9.3 % and no significant differences were present among the four strains ($p>0.05$).

Ultrastructural examination of the neuronal aggregates confirmed that most of the unmyelinated neurons within the clusters have characteristics of type I SGNs, such as round nuclei and mitochondria-rich cytoplasm (Figs. 2A,B). Within these clusters, the neurons were in direct somato-somatic apposition with no intervening Schwann cell or neural processes. Occasional junction-like structures appeared as electron-dense symmetrical patches on adjoining plasma membranes of neighboring neurons (Figs. 2C–F). Evidence of

morphological coupling structures in these unmyelinated neurons suggests these cells may be able to communicate with each other.

Neuronal degeneration in the basal turn

Although the majority of the neurons in the basal turn of Ly5.1 mice has the morphology of myelinated type I SGNs, electron micrographs revealed an abnormal appearance in some of these neurons in Ly5.1 mice (Fig. 3). The neuronal plasmalemma was detached from the myelin sheaths usually in one pole (Figs. 3A–C). Homeless Schwann cells and their processes were seen in the space between the neuronal cell bodies (Fig. 3A). A few abnormal myelinated type I neurons were also seen infrequently in the basal turn of C57BL/6J mice, but not in SJL/J and CBA/CaJ mice (data not shown). Morphometric analysis (Fig. 3E) revealed that SGN density in the basal turn of Ly5.1 mice was significantly less than that of C57BL/6J mice ($p < 0.01$). Note that cell density in Ly5.1 and C57BL/6J mice was normalized to that of CBA/CaJ mice.

Expression patterns of glial and neuronal markers

Further characterization of the unmyelinated neurons and neuronal aggregates was undertaken by labeling cryosections from Ly5.1, CBA/CaJ and C57BL/6J mice (Fig. 4) with antibodies directed against Schwann cells (CNPase) and neurons (TuJ1and NF 200). An antibody for Na,K-ATPase was also used. In the CBA/CaJ mouse cochleas, each TuJ1 positive neuron is encapsulated by a CNPase-positive myelin sheath resulting in a honeycomb–like staining pattern (Figs. 4A–C). In the apical and middle turns of the Ly5.1 mouse cochleas, the honeycombed pattern coalesced into several large units reflecting the loss of Schwann cell processes and myelin around individual neurons (Figs. 4D–F). The CNPase immunostaining data thus verified the morphological findings demonstrating a deficiency of Schwann cell processes in neuronal clusters in Ly5.1 mice in Figs. 1 and 2.

In Ly5.1 mice, the aggregated neurons stained positively for TuJ1, NF200 and Na, K-ATPase (Figs. 4–6). TuJ1 and NF200 are two well-characterized neural cell markers. Na, K-ATPase is essential for maintaining cellular ion concentration gradients and is of particular significance for neuronal cells that depend on it for repolarization after stimulation. The expression of TuJ1, NF200 and Na, K-ATPase in the aggregated neurons suggests that these unmyelinated neurons maintain many of their basic neuronal characteristics.

Expression pattern of connexin 29

Connexins are the major structural proteins in gap junctions, which allow direct metabolic and electrical communication between adjacent cells, including neurons and their supporting cells. Dual immunostaining of CBA/CaJ mouse cochleas revealed connexin 29-positive Schwann cell processes ensheathing NF 200-reactive SGNs in CBA/CaJ mice (Fig. 5A). In contrast, immunostaining for connexin 29 was mostly absent around the individual neurons forming neural clusters in Ly5.1 mice (Fig. 5C). However, strong staining for connexin 29 was present in almost all nerve processes within the osseous spiral lamina of Ly5.1 mice (Fig. 5D), with a distribution pattern similar to that in CBA/CaJ and C57BL/6J mice (data not shown). A deficiency of connexin 29 was also seen between aggregated neurons in the apical turn of C57BL/6J mice (Fig. 5B), but it was infrequent compared to that in Ly5.1 mice.

Although junction-like structures were present between the aggregated neurons (Fig. 2), no connexin 29 expression was seen between these unmyelinated neurons under observation with light microscopy (Fig. 5C). This result suggests that the connexin 29 is a fine structure protein that form gap junctions coupling a neuron and its Schwann cell, but are not the junction-like structures seen between unmyelinated neurons within the neuronal cluster.

Expression pattern of peripherin

To determine whether some of the unmyelinated neurons within the aggregated clusters are type II neurons, Ly5.1 mouse ears were dual-labeled for peripherin and NF 200 (Fig. 6). Data collected from about 40 randomly selected sections from five Ly5.1 mice revealed that only 6.8 % (47 of 696 neurons) of the total population of SGNs were peripherin-positive. Peripherin-positive cells had a similar distribution and frequency in the apical, middle and basal turns in Ly5.1 mice which matched that seen in all three control strains (data not shown). Thus, dual- immunostaining with peripherin and NF 200 confirmed that the majority of aggregated SGNs are type I cells.

Peripheral innervation and sensory hair cells

Confocal images of surface preparations stained with NF-200 allow visualization of only unmyelinated parts of nerve fibers in the rodent inner ear (Berglund and Ryugo et al., 1991; Lang et al., 2006b; Wise et al., 2005; McLean et al., 2009). All nerve processes of type I SGNs lose their myelin sheath prior to entering the organ of Corti through the habenula. The innervation pattern of the auditory nerve along the organ of Corti in all three turns of Ly5.1 mice does not differ from that previously described in normal inner ears of rodents (Fig. 7A; Wise et al., 2005; McLean et al., 2009).

Previous studies have documented that C57BL/6J mice suffer from hair cell degeneration beginning at about 1–2 month of age (Mikaelian et al., 1974). The survival of inner (IHCs) and outer hair cells (OHCs) in 1 to 1.5 month-old Ly5.1 and C57BL/6J mice was evaluated in surface preparations stained with myosin VII (Figs. 7B–D) and FITC-labeled phalloidin. A scattered loss of OHCs was observed in both Ly5.1 and C57BL/6 mice with no significant differences in OHC survival between the two strains (Fig. 7E; $p > 0.05$). No missing IHCs were seen in both Ly5.1or C57BL/6J mice (data not shown).

ABR thresholds, wave I latency and amplitude I/O functions

Mean ABR thresholds for 1 to 1.5 month-old CBA/CaJ (n=26), Ly5.1 (n= 21), C57BL/6J (n=20) and SJL/J (n=8) mice were shown in Figure 8. The CBA/CaJ mouse is considered the “gold standard” strain for maintaining excellent hearing throughout much of its life span (Henry and Chole 1980;Li and Borg 1991;Zheng et al., 1999). The C57BL/6J strain exhibits hearing loss beginning at an early age (Mikaelian et al., 1974;Henry and Chole, 1980). ABR thresholds in Ly5.1 mice are significantly higher than those of CBA/CaJ mice ($p < 0.01$). At frequencies below 32 kHz, ABR thresholds of Ly5.1 mice were similar to those of C57BL/6J and SJL/J mice. However, at frequencies higher than 32 kHz, ABR thresholds of Ly5.1 mice were mildly elevated compared to C57BL/6J and SJL/J mice ($p < 0.01$). The threshold shifts at higher frequencies in Ly5.1 mice support our findings of the loss of SGNs in the base of the cochlea in this strain (Fig. 3).

Mean ABR wave I latency versus intensity for Ly5.1 and C57BL/6J mice were plotted in Fig. 9. As shown in the Fig. 8, no significant difference in ABR thresholds at 5.6, 8, 16 and 22.6 kHz between the Ly5.1 and C57BL/6J mice allowed an effective comparison of the latency I/O functions between these two stains. A significant increase in wave I latencies was seen at 5.6 and 8 kHz in Ly5.1 mice, as compared to C57BL/6J mice (ANOVA, $p < 0.01$). The results were consistent with the presence of numerous unmyelinated SGNs in the apical and middle turns of Ly5.1 mice (Figs 1, 2), perhaps resulting in slower conduction velocities.

ABR wave I amplitude I/O functions allow examination of supra-threshold amplitudes to assess the gross activity of the primary auditory nerves at high signal levels. Amplitudes of ABR wave I were measured as the difference between the positive peak and the following

negative trough. Mean data for ABR wave I amplitude levels from Ly5.1 and C57BL/6J mice were plotted in Fig. 10. The ABR wave I amplitude I/O functions from Ly5.1 mice are flattened slightly at 8, 16 and 22.6 kHz compared to those of C57BL/6J mice. The flattened curves of wave I amplitude I/O functions suggest a functional decline of SGNs which may correlate to the loss of SGNs in the basal cochlea of Ly5.1 mice.

DISCUSSION

An unusual feature of the Ly5.1 mouse strain was the finding that a large percentage of SGNs in the apical and middle turns of the cochlea were unmyelinated. Most of these SGNs exhibited the characteristics of type I neurons and aggregated to form neural clusters. Interestingly, although ABR thresholds were similar in Ly5.1 and their background C57BL/6J strain, Ly5.1 mice had prolonged ABR wave I latencies at low and middle frequencies, a finding that may be related to the high level of unmyelinated SGN aggregation in the upper turns.

The integrity of the myelin sheath encasing a nerve fiber is important for proper function and, in some cases, for the survival of mature neurons. Myelin deficiency in the inner ear has been previously investigated in Tr^j, and '*bt*' mutant hamsters, P_0-DT-A transgenic mice and TMPRSS1-deficient mice (Zhou et al., 1995a; 1995b; Guipponi et al., 2007). The Tr^j hamster was created by a mutation of chromosome 11 in the peripheral myelin protein PMP-22 leading to its improper incorporation into the myelin (Suter et al., 1992). The '*bt*' hamster is another mutant model characterized by having a black coat and trembling of the trunk and hindquarters, although the specific mutation is unknown. In P_0-DT-A transgenic mice, the peripheral myelin protein P0 promoter was used to artificially introduce the gene encoding bacterial diphtheria toxin A chain (DT-A). Mice deficient for hepsin, also known as TMPRSS1, exhibit profound hearing loss with elevated hearing thresholds and decreased expression of the myelin basic protein and myelin protein zero. The pathology in the myelin-deficient animal models described above includes decreased dendritic density, thinner compact sheaths surrounding the axons and a slight decrease in the number of SGNs across all cochlear turns. Although, all these animals showed some loss of auditory function, the level of decline varied widely among the different models. Unlike these myelin-deficiency models, the morphological changes in Ly5.1 mice were mainly restricted to the lack of Schwann cell ensheathment and myelinization around the cell bodies of many type I SGNs. Although numerous unmyelinated neurons formed aggregated units in the apical and middle turns, there was little change in the appearance of the peripheral processes of these cells, almost all of which were heavily myelinated. Moreover, neural cell loss in Ly5.1 mice was limited to the basal turn.

The presence of unmyelinated neurons and neuronal aggregation has been reported in C57BL/6J mice (Cohen et al., 1990; Hequembourg and Liberman 2001; Ohlemiller and Gagnon 2004). The overall incidence of this phenomenon appears to increase with advancing age. However, unlike the previous findings in C57BL/6J mice, the much greater level of neuronal aggregation in Ly5.1 mice does not appear to be an age-related degenerative phenomenon, but rather appears to result from a developmental deficiency in myelinization. Even though a large percentage of SGNs in the apical and middle turns of Ly5.1 mice were unmyelinated, overall neural density in these regions did not differ significantly from that in the control mouse strains. In addition, no evidence of neural or Schwann cell degeneration was seen in the apical and middle turns of Ly5.1 mice. Furthermore, the features of aggregated neuronal clusters did not differ between 8 month-old and 1 month-old Ly5.1 mice (Supplementary Fig. 2). Thus, it is unlikely that the neuronal clusters seen in the upper turns were formed by 'clumping' of degenerative type I SGN cell bodies. Although no degenerative changes were seen in upper turns of Ly5.1 mice, we did

observe histopathological changes consistent with early degeneration in myelinated type I SGNs in the basal turn of this strain. However, no neural aggregates were seen in the basal turn of Ly5.1 mice suggesting that the affected SGNs in this location underwent complete degeneration. This supposition is consistent with our quantitative data demonstrating a reduced neural density in the spiral ganglion of Ly5.1 mice. It is possible to speculate that the increased ABR thresholds at frequencies above 32 kHz in Ly5.1 mice are related to the loss of SGNs in the base of the cochlea in the strain.

Gap junctions are channels in the plasma membranes of adjacent cells that allow ions and small molecules to diffuse from cell to cell. These channels are primarily composed of proteins termed connexins. To date, about 20 connexin genes have been reported in rodents, each of which is expressed differentially in various tissues and cell types (Willecke et al., 2002). Connexin 29 has been shown to be highly expressed in Schwann cells in the spiral ganglion (Tang et al., 2006). Double staining for connexin 29 with a neural marker confirmed our morphological observations demonstrating the absence of Schwann cell processes and myelin sheaths within neural clusters in Ly5.1 and C57BL/6J mice. These data point to a defect of the Schwann cells or SGNs that results in incomplete myelination of SGNs in the upper turns of Ly5.1 mice. The fact that development of the cochlea begins in the upper basal turn and proceeds apically suggests strongly that this is a developmental problem.

Neural aggregation and coupling have been reported previously in several regions of the central nervous system including the avian suprachiasmatic and preoptic regions, auditory field L of the neostriatum in the starling, the auditory cortex in the cat and the striatum in the rat (Oksche et al., 1974; Antonova 1975; Saini and Leppelsack 1977; Paskevich et al., 1991). Electron microscopy studies demonstrated that neurons within clusters made direct contact via specialized junction-like symmetrical structures in the rat stratum and the avian ciliary ganglion (Cantino and Mugnaini 1975; Saini and Leppelsack 1977). These specialized junction-like structures were similar to those observed here in the spiral ganglia of Ly5.1 mice (Fig. 2). The appearance of specialized junction-like zones between the aggregated neurons supports the possibility of direct cell-to-cell communication occurring among these neurons. If so, communication among these aggregated neurons would allow each neural cluster to act as a “functional unit”. However, how this would affect auditory information processing remains undetermined.

Unlike most mammalian species, the cell bodies of most human spiral ganglion neurons are unmyelinated as demonstrated by light and electron microscopic studies (Kimura et al., 1979; Ota and Kimura 1980; Arnold 1987; Nadol 1988; Tylstedt et al., 1997; Rask-Andersen et al., 2000; Glueckert et al., 2005). These findings have prompted speculation that a slower neural conduction rate may exist in humans compared to other mammalian species. Although the precise timing of myelination of spiral ganglion cell bodies in the developmental human ear remains unknown, a light microscopic study of human embryos, fetuses and a one-day-old neonate suggested that SGN myelination begins around 13 weeks (74 mm crl fetus) from basal spiral ganglion and moves apicalwards (Sánchez et al., 1995). A large number (about 94 %) of the unmyelinated SGNs were found in human ears aged 9 months to 92 years (Ota and Kimura 1980). Interestingly, this study has also noted a characteristic clustering of unmyelinated SGNs in both normal young adult and aged human temporal bones. These “structural units” in the human temporal bone have several features in common with the aggregated neural clusters observed in Ly5.1 mice. These similarities include 1) the neurons within the clusters are mostly unmyelinated and are not separated by intervening Schwann cell processes; 2) junction-like structures are present between the neighboring neurons within neural clusters; and 3) neural clusters are commonly present in the apical and middle turns, but not in the basal turn (Spoendlin and Schrott 1990; Tylstedt

and Rask-Andersen 2001; Glueckert et al., 2005). Even though the functional characteristics of neural clusters and the intercellular contacts between unmyelinated neurons remain unknown, the finding of “structural units” in the human spiral ganglion suggests the existence of “functional units”, which may play a principal role in generating synchronous activity and coding complex speech signals (Glueckert et al., 2005). To our knowledge, the Ly5.1 mouse strain is the only rodent model reported to have a large number of “human-like SGN” elements. This mouse strain may thus provide a useful model for studying the mechanisms of synchronous neural activity and other auditory response properties in humans.

Supplementary Material

Refer to Web version on PubMed Central for supplementary material.

Acknowledgments

The authors thank Dr. Kelly C. Harris, Ms. Nancy M Smythe, Ms. Juhong Zhu, and Mr. James Nicholson for their assistance in auditory functional and histological assays, Drs. Bernd Fritzsch and Edwin W. Rubel for their critical comments and invaluable discussion over the course of this study.

Grant sponsor: National Institutes of Health; Grant number: DC00422 (H.L.); Grant number: DC07506 (H.L.); Grant number: DC00713 (B.A.S.); Office of Research & Development, Medical Research Services, Department of Veterans Affairs (A.C.L.); American Academy of Otolaryngology-Head and Neck Surgery; Grant number: CORE 130165 (L.K.).

LITERATURE CITED

Antonova AM. The spatial organization of cat auditory cortex neuronal assemblies. Arkh Anat Gistol Embriol. 1975; 68(1):73–78. [PubMed: 1131020]

Arnold W. Myelination of the human spiral ganglion. Acta Otolaryngol Suppl. 1987; 436:76–84. [PubMed: 3478961]

Avraham KB, Hasson T, Steel KP, Kingsley DM, Russell LB, Mooseker MS, Copeland NG, Jenkins NA. The mouse Snell's waltzer deafness gene encodes an unconventional myosin required for structural integrity of inner ear hair cells. Nat Genet. 1995; 11(4):369–375. [PubMed: 7493015]

Berglund AM, Ryugo DK. Neurofilament antibodies and spiral ganglion neurons of the mammalian cochlea. J Comp Neurol. 1991; 306(3):393–408. [PubMed: 1865000]

Cantino D, Mugnaini E. The structural basis for electrotonic coupling in the avian ciliary ganglion. A study with thin sectioning and freeze-fracturing. J Neurocytol. 1975; 4(5):505–536. [PubMed: 1176998]

Charbonneau H, Tonks NK, Walsh KA, Fischer EH. The leukocyte common antigen (CD45): a putative receptor-linked protein tyrosine phosphatase. Proc Natl Acad Sci U S A. 1988; 85(19): 7182–7186. [PubMed: 2845400]

Cohen GM, Park JC, Grasso JS. Comparison of demyelination and neural degeneration in spiral and Scarpa's ganglia of C57BL/6 mice. J Electron Microsc Tech. 1990; 15:165–172. [PubMed: 2355267]

Ding, D.; McFadden, SL.; Salvi, RJ. Handbook of mouse auditory research. Willott, JF., editor. New York: CRC; 2001. p. 189-204.

Dunah AW, Hueske E, Wyszynski M, Hoogenraad CC, Jaworski J, Pak DT, Simonetta A, Liu G, Sheng M. LAR receptor protein tyrosine phosphatases in the development and maintenance of excitatory synapses. Nat Neurosci. 2005; 8(4):458–467. [PubMed: 15750591]

Ehret, G. Peripheral anatomy and physiology II. In: Willott, JF., editor. The auditory psychology of the mouse. Springfield, IL: Charles C. Thomas; 1983. p. 169-200.

Fishman GI, Spray DC, Leinwand LA. Molecular characterization and functional expression of the human cardiac gap junction channel. J Cell Biol. 1990; 111(2):589–598. [PubMed: 1696265]

Glueckert R, Pfaller K, Kinnefors A, Rask-Andersen H, Schrott-Fischer A. The human spiral ganglion: new insights into ultrastructure, survival rate and implications for cochlear implants. Audiol Neurootol. 2005; 10(5):258–273. [PubMed: 15925863]

Gorham JD, Baker H, Kegler D, Ziff EB. The expression of the neuronal intermediate filament protein peripherin in the rat embryo. Brain Res Dev Brain Res. 1990; 57:235–248.

Gubbels SP, Woessner DW, Mitchell JC, Ricci AJ, Brigande JV. Functional auditory hair cells produced in the mammalian cochlea by in utero gene transfer. Nature. 2008; 455(7212):537–541. [PubMed: 18754012]

Guillery RW. On counting and counting errors. J Comp Neurol. 2002; 447(1):1–7. [PubMed: 11967890]

Guipponi M, Tan J, Cannon PZ, Donley L, Crewther P, Clarke M, Wu Q, Shepherd RK, Scott HS. Mice deficient for the type II transmembrane serine protease, TMPRSS1/hepsin, exhibit profound hearing loss. Am J Pathol. 2007; 171(2):608–616. [PubMed: 17620368]

Hafidi A. Peripherin-like immunoreactivity in type II spiral ganglion cell body and projections. Brain Res. 1998; 805(1–2):181–190. [PubMed: 9733963]

Hequembourg S, Liberman MC. Spiral ligament pathology: a major aspect of age-related cochlear degeneration in C57BL/6 mice. J Assoc Res Otolaryngol. 2001; 2:118–129. [PubMed: 11550522]

Henry KR, Chole RA. Genotypic differences in behavioral, physiological and anatomical expressions of age-related hearing loss in the laboratory mouse. Audiology. 1980; 19(5):369–383. [PubMed: 7436856]

Hildebrand C, Remahl S, Persson H, Bjartmar C. Myelinated nerve fibres in the CNS. Prog Neurobiol. 1993; 40(3):319–384. [PubMed: 8441812]

Jagger DJ, Housley GD. Membrane properties of type II spiral ganglion neurones identified in a neonatal rat cochlear slice. J Physiol. 2003; 552(Pt 2):525–533. [PubMed: 14561834]

Jones SM, Jones TA, Johnson KR, Yu H, Erway LC, Zheng QY. A comparison of vestibular and auditory phenotypes in inbred mouse strains. Brain Res. 2006; 1091:40–46. [PubMed: 16499890]

Johnson KG, Van Vactor D. Receptor protein tyrosine phosphatases in nervous system development. Physiol Rev. 2003; 83(1):1–24. [PubMed: 12506125]

Kiang NY, Rho JM, Northrop CC, Liberman MC, Ryugo DK. Hair-cell innervation by spiral ganglion cells in adult cats. Science. 1982; 17:175–177. [PubMed: 7089553]

Kim SU, McMorris FA, Sprinkle TJ. Immunofluorescence demonstration of 2':3'-cyclic-nucleotide 3'-phosphodiesterase in cultured oligodendrocytes of mouse, rat calf and human. Brain Res. 1984; 300(1):195–199. [PubMed: 6329429]

Kimura RS, Ota CY, Takahashi T. Nerve fiber synapses on spiral ganglion cells in the human cochlea. Ann Otol Rhinol Laryngol Suppl. 1979; 88(6 Pt 3 Suppl 62):1–17. [PubMed: 118697]

Lang H, Schulte BA, Schmiedt RA. Ouabain induces apoptotic cell death in type I spiral ganglion neurons, but not type II neurons. J Assoc Res Otolaryngol. 2005; 6(1):63–74. [PubMed: 15735933]

Lang H, Ebihara Y, Schmiedt RA, Minamiguchi H, Zhou D, Smythe N, Liu L, Ogawa M, Schulte BA. Contribution of bone marrow hematopoietic stem cells to adult mouse inner ear: mesenchymal cells and fibrocytes. J Comp Neurol. 2006a; 496:187–201. [PubMed: 16538683]

Lang H, Schulte BA, Zhou D, Smythe N, Spicer SS, Schmiedt RA. Nuclear factor kappaB deficiency is associated with auditory nerve degeneration and increased noise-induced hearing loss. J Neurosci. 2006b; 26:3541–3550. [PubMed: 16571762]

Lang H, Schulte BA, Goddard JC, Hedrick M, Schulte JB, Wei L, Schmiedt RA. Transplantation of mouse embryonic stem cells into the cochlea of an auditory-neuropathy animal model: effects of timing after injury. J Assoc Res Otolaryngol. 2008; 9:225–240. [PubMed: 18449604]

Lee MK, Rebhun LI, Frankfurter A. Posttranslational modification of class III beta-tubulin. Proc Natl Acad Sci U S A. 1990; 87(18):7195–7199. [PubMed: 2402501]

Li HS, Borg E. Age-related loss of auditory sensitivity in two mouse genotypes. Acta Otolaryngol. 1991; 111(5):827–834. [PubMed: 1759567]

McGuirt JP, Schulte BA. Distribution of immunoreactive alpha- and beta-subunit isoforms of Na,K-ATPase in the gerbil inner ear. J Histochem Cytochem. 1994; 42:843–853. [PubMed: 8014467]

McLean WJ, Smith KA, Glowatzki E, Pyott SJ. Distribution of the Na,K-ATPase alpha subunit in the rat spiral ganglion and organ of corti. J Assoc Res Otolaryngol. 2009; 10:37–49. [PubMed: 19082858]

Mikaelian DO, Warfield D, Norris O. Genetic progressive hearing loss in the C57-b16 mouse. Relation of behavioral responses to chochlear anatomy. Acta Otolaryngol. 1974; 77(5):327–334. [PubMed: 4835632]

Nadol JB Jr. Comparative anatomy of the cochlea and auditory nerve in mammals. Hear Res. 1988; 34(3):253–266. [PubMed: 3049492]

Ohlemiller KK, Gagnon PM. Apical-to-basal gradients in age-related cochlear degeneration and their relationship to "primary" loss of cochlear neurons. J Comp Neurol. 2004; 479:103–116. [PubMed: 15389608]

Oksche A, Kirschstein H, Hartwig HG, Oehmke HJ, Farner DS. Secretory parvocellular neurons in the rostral hypothalamus and in the tuberal complex of Passer domesticus. Cell Tissue Res. 1974; 149(3):363–370. [PubMed: 4426070]

Ota CY, Kimura RS. Ultrastructural study of the human spiral ganglion. Acta Otolaryngol. 1980; 89(1–2):53–62. [PubMed: 7405577]

Paskevich PA, Evans HK, Domesick VB. Morphological assessment of neuronal aggregates in the striatum of the rat. J Comp Neurol. 1991; 305(3):361–369. [PubMed: 1709952]

Rask-Andersen H, Tylstedt S, Kinnefors A, Illing R. Synapses on human spiral ganglion cells: a transmission electron microscopy and immunohistochemical study. Hear Res. 2000; 141(1–2):1–11. [PubMed: 10713490]

Reid MA, Flores-Otero J, Davis RL. Firing patterns of type II spiral ganglion neurons in vitro. J Neurosci. 2004; 24(3):733–742. [PubMed: 14736859]

Richardson GP, Forge A, Kros CJ, Fleming J, Brown SD, Steel KP. Myosin VIIA is required for aminoglycoside accumulation in cochlear hair cells. J Neurosci. 1997 Dec 15; 17(24):9506–9519. [PubMed: 9391006]

Romand MR, Romand R. Development of spiral ganglion cells in mammalian cochlea. J Electron Microsc Tech. 1990; 15:144–154. [PubMed: 2355266]

Saga Y, Tung JS, Shen FW, Boyse EA. Alternative use of 5' exons in the specification of Ly-5 isoforms distinguishing hematopoietic cell lineages. Proc Natl Acad Sci U S A. 1987; 84:5364–5368. [PubMed: 3037546]

Saini KD, Leppelsack HJ. Neuronal arrangement in the auditory field L of the neostriatum of the starling. Cell Tissue Res. 1977; 176(3):309–316. [PubMed: 832299]

Sánchez Del Rey A, Sánchez Fernández JM, Martínez Ibarguen A, Santaolalla Montoya. Morphologic and morphometric study of human spiral ganglion development. Acta Otolaryngol. 1995; 115(2): 211–217. [PubMed: 7610807]

Schulte BA, Adams JC. Distribution of immunoreactive Na+,K+-ATPase in gerbil cochlea. J Histochem Cytochem. 1989; 37:127–134. [PubMed: 2536055]

Sekerková G, Zheng L, Mugnaini E, Bartles JR. Espin actin-cytoskeletal proteins are in rat type I spiral ganglion neurons and include splice-isoforms with a functional nuclear localization signal. J Comp Neurol. 2008; 509:661–676. [PubMed: 18551532]

Shen FW, Saga Y, Litman G, Freeman G, Tung JS, Cantor H, Boyse EA. Cloning of Ly-5 cDNA. Proc Natl Acad Sci U S A. 1985; 82(21):7360–7363. [PubMed: 3864163]

Siegel GJ, Holm C, Schreiber JH, Desmond T, Ernst SA. Purification of mouse brain (Na+ + K+)-ATPase catalytic unit, characterization of antiserum, and immunocytochemical localization in cerebellum, choroid plexus, and kidney. J Histochem Cytochem. 1984 Dec; 32(12):1309–1318. [PubMed: 6094658]

Spoendlin H. Innervation patterns in the organ of corti of the cat. Acta Otolaryngol. 1969; 67:239–254. [PubMed: 5374642]

Spoendlin H, Schrott A. Quantitative evaluation of the human cochlear nerve. Acta Otolaryngol Suppl. 1990; 470:61–69. discussion 69–70. [PubMed: 2239235]

Sprinkle TJ. 2',3'-cyclic nucleotide 3'-phosphodiesterase, an oligodendrocyte-Schwann cell and myelin-associated enzyme of the nervous system. Crit Rev Neurobiol. 1989; 4:235–301. [PubMed: 2537684]

Stepanek L, Stoker AW, Stoeckli E, Bixby JL. Receptor tyrosine phosphatases guide vertebrate motor axons during development. J Neurosci. 2005; 25(15):3813–3823. [PubMed: 15829633]

Suter U, Moskow JJ, Welcher AA, Snipes GJ, Kosaras B, Sidman RL, Buchberg AM, Shooter EM. A leucine-to-proline mutation in the putative first transmembrane domain of the 22-kDa peripheral myelin protein in the trembler-J mouse. Proc Natl Acad Sci U S A. 1992; 89(10):4382–4386. [PubMed: 1374899]

Tang W, Zhang Y, Chang Q, Ahmad S, Dahlke I, Yi H, Chen P, Paul DL, Lin X. Connexin29 is highly expressed in cochlear Schwann cells, and it is required for the normal development and function of the auditory nerve of mice. J Neurosci. 2006; 26:1991–1999. [PubMed: 16481432]

Tylstedt S, Rask-Andersen H. A 3-D model of membrane specializations between human auditory spiral ganglion cells. J Neurocytol. 2001; 30(6):465–473. [PubMed: 12037463]

Tylstedt S, Kinnefors A, Rask-Andersen H. Neural interaction in the human spiral ganglion: a TEM study. Acta Otolaryngol. 1997; 117(4):505–512. [PubMed: 9288204]

Weisz C, Glowatzki E, Fuchs P. The postsynaptic function of type II cochlear afferents. Nature. 2009 Oct 22; 461(7267):1126–1129. [PubMed: 19847265]

Willecke K, Eiberger J, Degen J, Eckardt D, Romualdi A, Güldenagel M, Deutsch U, Söhl G. Structural and functional diversity of connexin genes in the mouse and human genome. Biol Chem. 2002; 383(5):725–737. [PubMed: 12108537]

Wise AK, Richardson R, Hardman J, Clark G, O'leary S. Resprouting and survival of guinea pig cochlear neurons in response to the administration of the neurotrophins brain-derived neurotrophic factor and neurotrophin-3. J Comp Neurol. 2005; 487:147–165. [PubMed: 15880560]

Zebedee SL, Barritt DS, Raschke WC. Comparison of mouse Ly5a and Ly5b leucocyte common antigen alleles. Dev Immunol. 1991; 1(4):243–254. [PubMed: 1822988]

Zheng QY, Johnson KR, Erway LC. Assessment of hearing in 80 inbred strains of mice by ABR threshold analyses. Hear Res. 1999; 130(1–2):94–107. [PubMed: 10320101]

Zhou R, Assouline JG, Abbas PJ, Messing A, Gantz BJ. Anatomical and physiological measures of auditory system in mice with peripheral myelin deficiency. Hear Res. 1995a; 88(1–2):87–97. [PubMed: 8576008]

Zhou R, Abbas PJ, Assouline JG. Electrically evoked auditory brainstem response in peripherally myelin-deficient mice. Hear Res. 1995b; 88(1–2):98–106. [PubMed: 8576009]

Zhou X, Jen PH, Seburn KL, Frankel WN, Zheng QY. Auditory brainstem responses in 10 inbred strains of mice. Brain Res. 2006; 1091:16–26. [PubMed: 16516865]

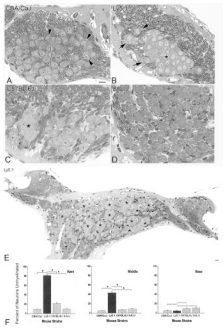

Figure 1. Morphological and quantitative evaluation of SGNs

A. SGNs in the apical turn of a young adult CBA/CaJ mouse. The majority of neurons are myelinated type I (I) neurons, which can be distinguished from type II (arrowheads) neurons by their round nucleus and darker cytoplasm. The perikaryon of type I cells is surrounded by a dark line, which represents the myelin sheath. Type II neurons are of smaller size, have lighter cytoplasm and eccentric nuclei, and are located near the root of the osseous spiral lamina or close to the intra-ganglionic spiral bundle. Note that few neurons are in direct contact with each other. Most neurons are separated by extracellular space or nerve fibers. **B. SGNs in the apical turn of an Ly5.1 mouse.** The majority of neurons are unmyelinated and grouped together as a cluster (*). The aggregated neurons have round nuclei, dark cytoplasm and lack a myelin sheath. No myelinated nerve fibers are visible within the clusters. Three myelinated type I neurons (arrows) are located at the periphery of the neuronal cluster. **C. SGNs in the apical turn of a C57BL/6J mouse.** A small cluster of eight unmyelinated neurons (*) is located on the left side of the section. Somata of these unmyelinated cells are clumped as shown in Fig.1B. Note the numerous normal-appearing myelinated type I neurons scattered in other areas of Rosenthal's canal. **D. SGNs in the apical turn of a SJL/J mouse.** The majority of neurons are myelinated type I neurons. No neural aggregation was seen in this strain. **E. Unmyelinated and aggregated neurons in the apical (right side) and middle (left side) turns from an Ly5.1 mouse**. The neural clusters are indicated with asterisks. The myelinated fibers in the osseous spiral lamina (osl) appear normal. **F. Mean percentages of unmyelinated neurons in the apical, middle and basal turns of CBA/CaJ, Ly5.1, C57BL/6J and SJL/J mice.** Unmyelinated cells comprise about 80% of SGNs in the apical turn and 40% of SGNs in the middle turn of Ly5.1 mice. Differences in the percentage of unmyelinated neurons between the Ly5.1 and the other three strains are statistically significant in the apical and middle turns ($p < 0.01$). Scale bars: **A–D**, 10 μm; **E**, 20 μm.

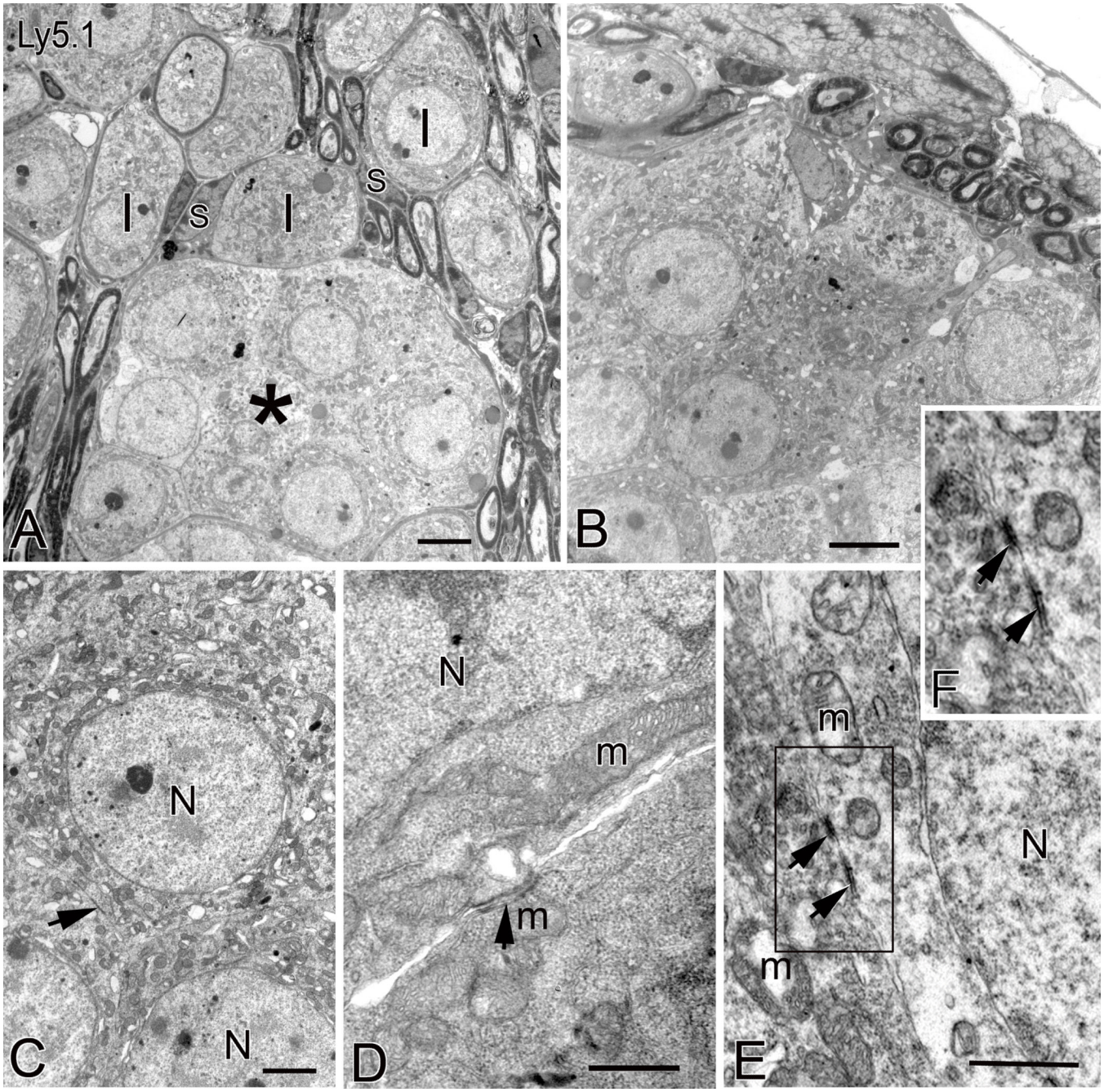

Figure 2. Ultrastructure of neural clusters in Ly5.1 mice

A. Aggregated unmyelinated SGNs in the middle turn form a cluster (*) with a common myelin sheath. Neurons within the cluster have round nuclei and mitochondria-rich cytoplasm. Several normal-appearing myelinated type I SGNs (I) separated by Schwann cells (S) and neural processes occupy the region above the cluster. **B. Neural cluster in the apical turn of another Ly5.1 mouse.** Note that several nerve fibers appear outside the neural cluster. **C. Aggregated unmyelinated neurons with large round nuclei (N).** Their perikarya are directly in contact with one another. A black arrow points to a specialized membrane structure between neighboring cells. **D.** and **E. Higher magnification images of somato-somatic apposition revealing junction-like symmetrical structures.** The arrows

point to the dark patches on the adjoining plasma membranes of two neighboring neurons. **F. Enlarged image of corresponding boxed area in Fig. 2E.** m, mitochondria. Scale bars: **A** and **B**, 2.5 μm; **C**, 1.5 μm; **D** and **E**, 500 nm.

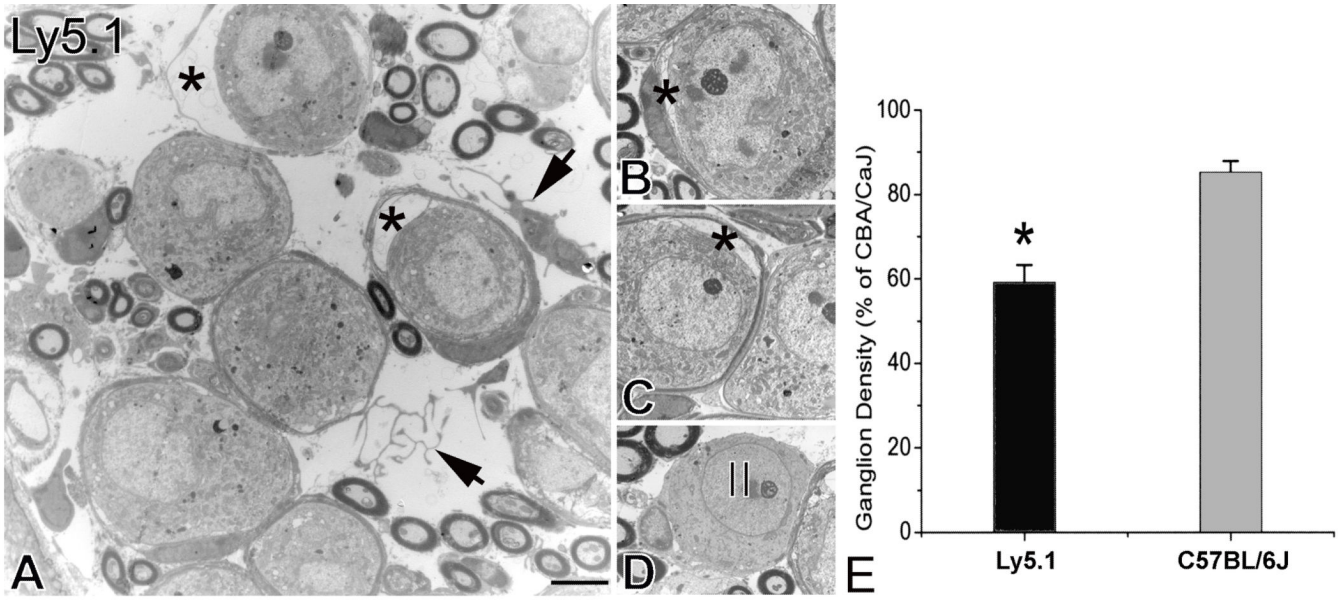

Figure 3. Neural loss in the basal turn of Ly5.1 mice

A. Histopathological changes in the spiral ganglion. Two neurons have apparently separated from their surrounding myelin sheath (*). A homeless Schwann cell and Schwann cell processes appear within the extracellular space (arrows). **B** and **C. Separation of Schwann cells from type I neurons (*).** The neurons were in the basal turn taken from another Ly5.1 mouse. **D. Type II neuron in the basal turn**. The image was taken from the same mouse shown in Figs. **3B** and **C**. Note that non-myelinating Schwann cells appear around the neuron. **E. Mean ganglion cell density in the basal turn of Ly5.1 and C57BL/6J mice expressed as a percent of that in CBA/CaJ mice.** The loss of SGNs in Ly5.1 mice is significant ($p < 0.01$). Scale bars: **A–D**, 2.5 μm.

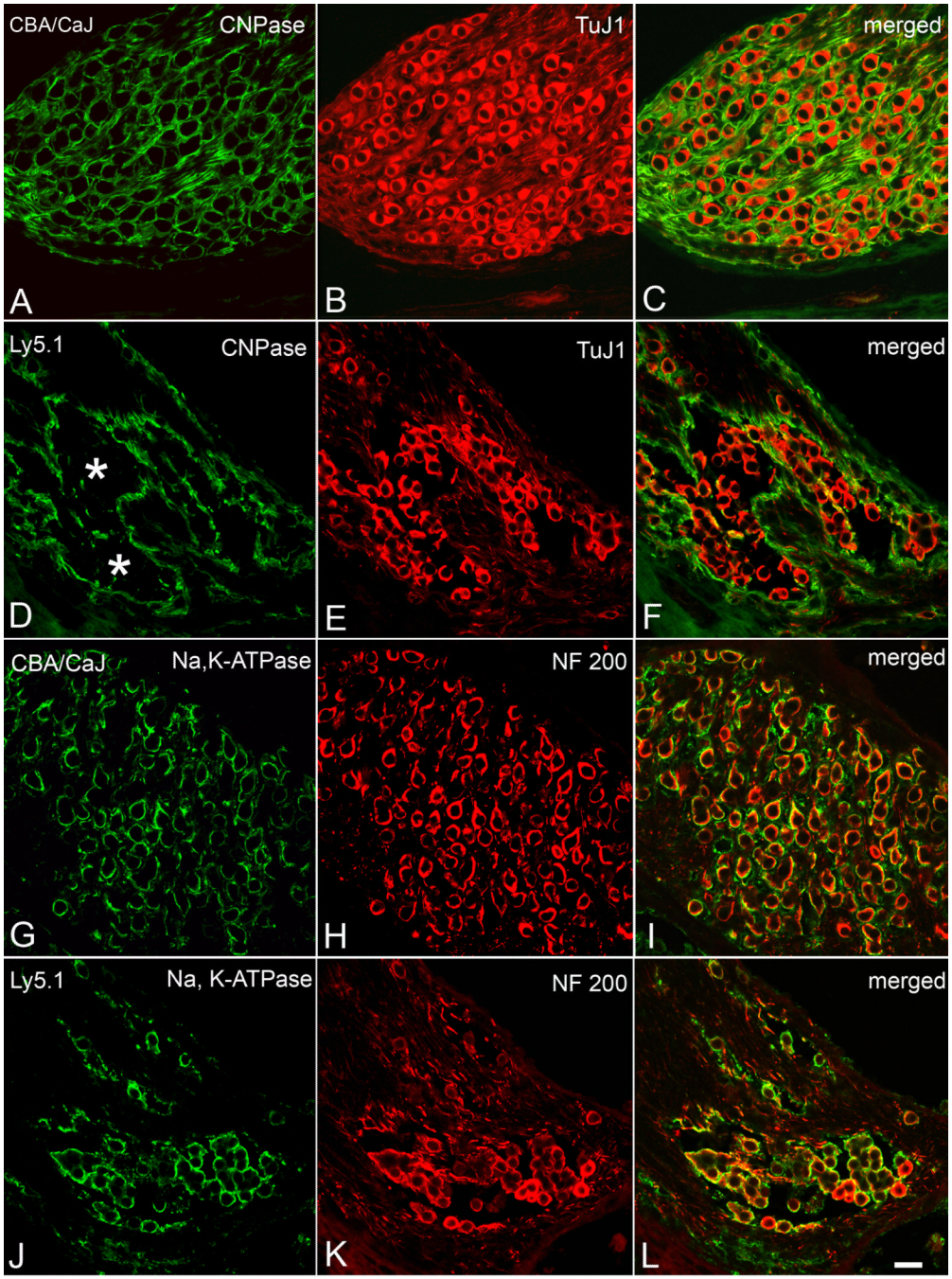

Figure 4. Immunostaining for neuronal and glial markers in apical turns from a CBA/CaJ and an Ly5.1 mouse

A–C. Dual labeling with anti-CNPase (green) and anti-TuJ1 III β-tubulin (red) in a CBA/CaJ mouse. TuJ1 antibody preferentially labels the cytoplasm of large type I neurons (Sekerkova et al., 2008). CNPase labeling of Schwann cells and their myelin sheaths results in a honeycomb-like pattern in the SG. **D–F. Dual labeling with anti-CNPase (green) and anti-TuJ1 III β-tubulin (red) in an Ly5.1 mouse.** The honeycomb-like pattern is completely disrupted in the apical turn. Most SGNs lacking a CNPase-positive myelin sheath stained positively for TuJ1. **G–I. Dual labeling with anti-Na, K-ATPase (green) and anti-neurofilament 200 (NF 200, red) in a CBA/CaJ mouse.** Strong surface staining

for Na, K-ATPase is seen in most of the SGNs **J–L. Dual labeling with anti-Na, K-ATPase (green) and anti-neurofilament 200 (NF 200, red) in an Ly5.1 mouse.** Again, most NF200-positive neurons were co-labeled with Na, K-ATPase. Scale bar: **A–L**, 25 μm. A magenta-green copy of this figure is available as Supplementary Figure 3.

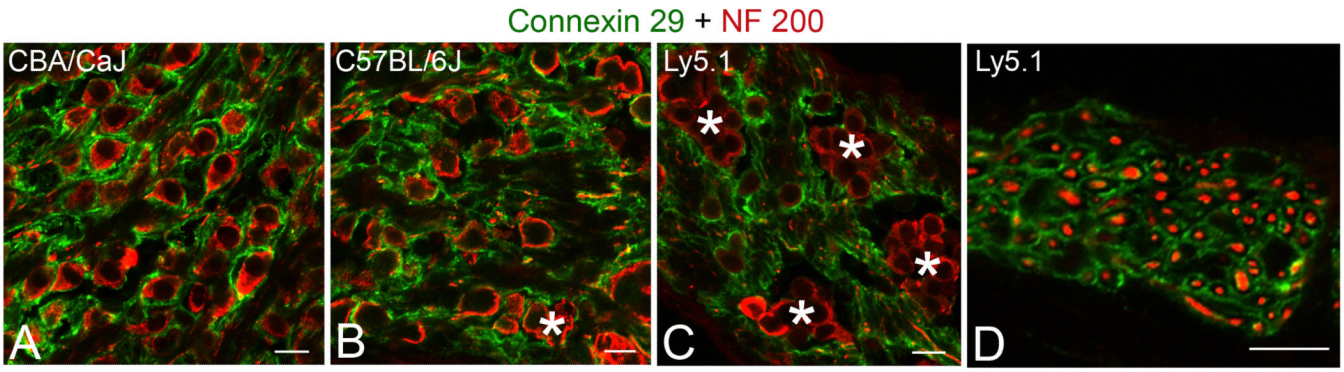

Figure 5. Immunostaining for connexin 29. A–D. Dual labeling with connexin 29 (green) and NF 200 (red) in the sections from apical turns

Schwann cells and their processes ensheathing neurons stain positively for connexin 29 in a CBA/CaJ mouse. In contrast, staining for connexin 29 is lacking around the neurons within a small neural cluster (*) in a C57BL/6J mouse (**B**) as well as in neurons within four neural clusters (*) in an Ly5.1 mouse (**C**). NF200-positive myelinated nerve fibers (red) are surrounded by connexin 29-positive Schwann cell processes in the osseous spiral lamina of an Ly5.1 mouse (**D**). Scale bar: **A–D**, 10 μm. A magenta-green copy of this figure is available as Supplementary Figure 4.

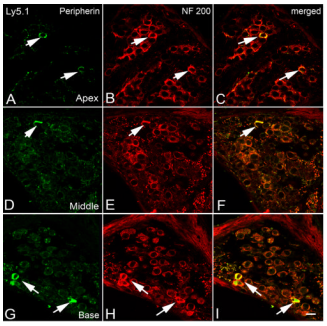

Figure 6. Dual immunolabeling for peripherin (green) and NF 200 (red) in the apical (A–C), middle (D–F) and basal turn (G–I) of an Ly5.1 mouse

Neurons expressing both peripherin and NF 200 (arrows) are considered to be type II SGNs and are scattered along the periphery of Rosenthal's canal. Scale bar: A–I, 10 μm. A magenta-green copy of this figure is available as Supplementary Figure 5.

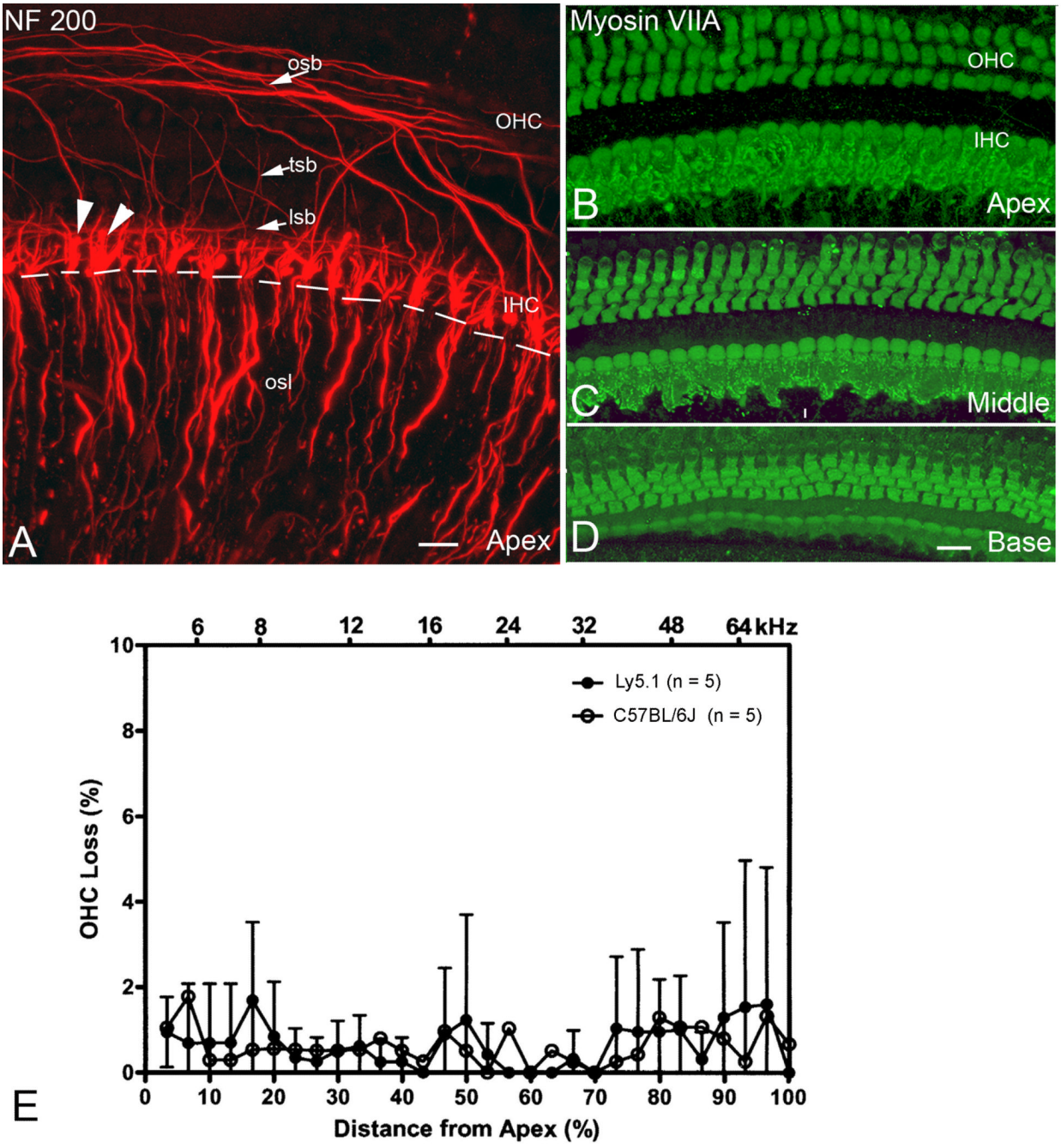

Figure 7. Cochlear innervation patterns and sensory hair cells

A. Surface preparation from the apical turn of an Ly 5.1 mouse stained with NF 200. NF 200 positive nerve processes project to both inner (IHC) and outer (OHC) hair cells. Note that unmyelinated nerve processes distal to the habenula perforata (white dashed line) were labeled, whereas myelinated nerve fibers within the osl, proximal to the habenula perforata, were unlabeled. NF 200 positive fibers include large terminals (arrowheads) under IHCs, the inner spiral bundle (isb), the tunnel spiral bundle (tsb), the tunnel radial bundle (trb) and the outer spiral bundle (osb). **B–D. Surface preparations from the apical, middle and basal turns of an Ly5.1 mouse stained with myosin VIIA. Almost all** IHCs and OHCs were intact. **E. Mean cochleograms from C57BL/6J and Ly 5.1 mice.** Very little

OHC loss was seen in either strain. Data presented as mean ± standard error of the mean (SEM) (n=5 per group). A magenta-green copy of this figure is available as Supplementary Figure 6. Scale bars: **A**, 15 μm; **B–D**, 20 μm.

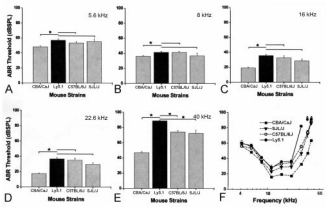

Figure 8. Comparisons of ABR thresholds obtained from CBA/CaJ, Ly5.1, C57BL/6J and SJL/J mice at 5.6 (A), 8 (B), 16 (C), 22.6 (D) and 40 (E) kHz

All data are presented as mean ± SEM. Asterisks indicate statistically significant differences at the indicated frequency ($p<0.01$). No significant differences were seen at frequencies lower than 22.6 kHz in ABR thresholds of Ly5.1 mice compared to C57BL/6J and SJL/J mice. Significant threshold differences at 40 kHz between Ly5.1 and the other three strains tested. **F. Mean ABR thresholds at all frequencies tested.** Thresholds are elevated by 7–45 dB across tested frequencies compared to those of CBA/CaJ mice.

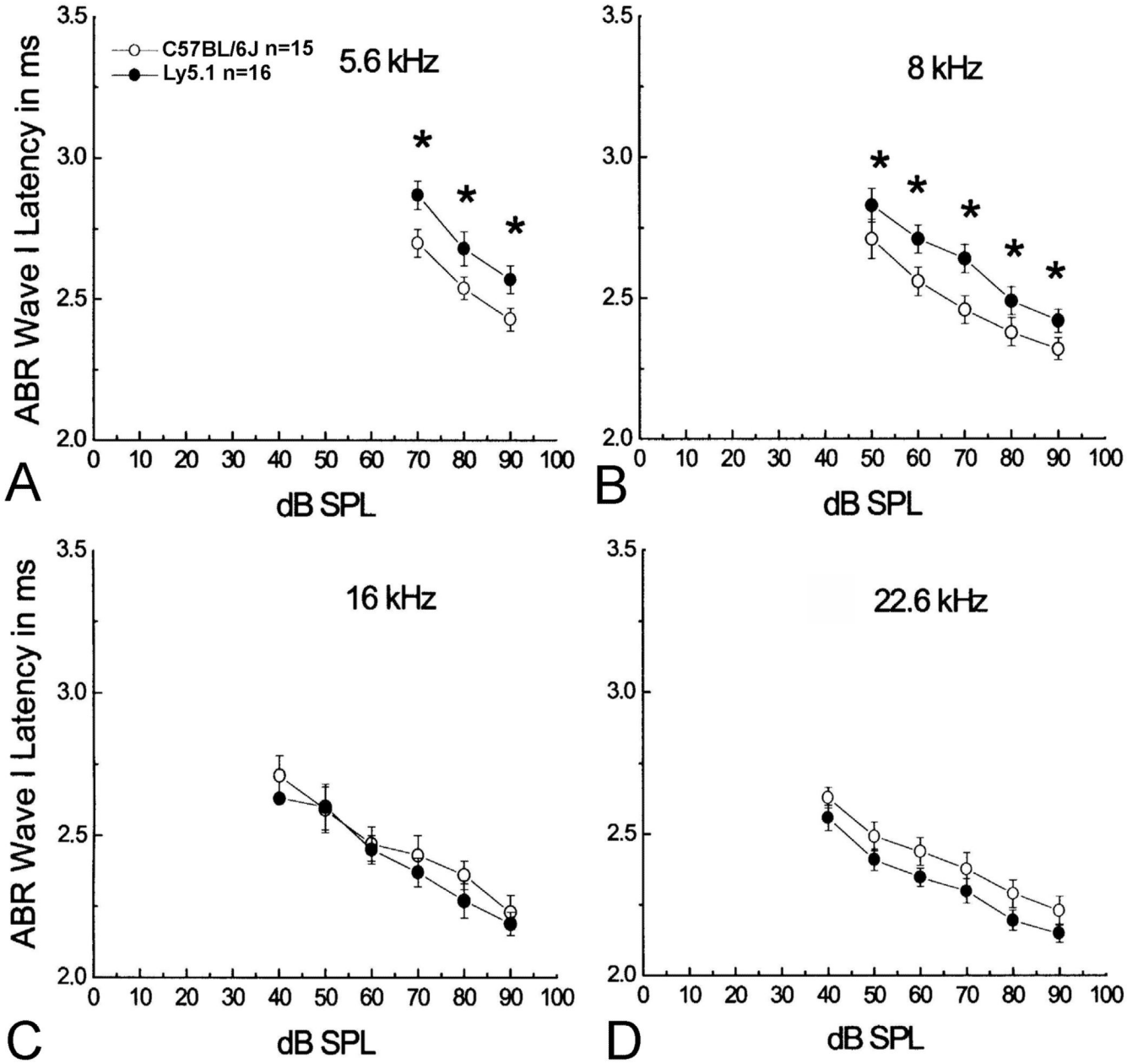

Figure 9. Mean wave I latency vs. level functions

Delayed wave I latencies in Ly5.1 mice at 5.6 (A) and 8 kHz (B), but not at 16 (C) and 22.6 kHz (D) compared to those of C57BL/6J mice. Data are presented as mean ± standard error of the mean (SEM). Asterisks indicate a statistically significant difference at the indicated frequency ($p<0.01$).

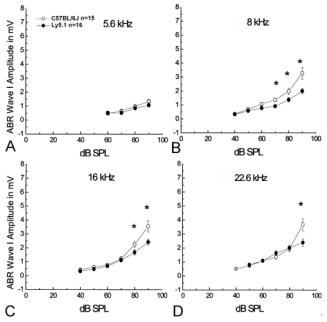

Figure 10. Mean wave I amplitudes vs. level functions

Decreased wave I amplitude at 8 (B), 16 (C) and 22.6 (D) kHz with high levels of stimuli compared to C57BL/6J mice. Note that no significant decrease was seen between Ly5.1 and C57BL/6J mice in wave I amplitude at 5.6 kHz (**A**). The flattened curves of wave I amplitude I/O functions suggest a functional decline of SGNs which may correlate to the lower density of neurons in the basal cochlea of Ly5.1 mice (Fig. 3). Data were collected from the mice shown in Figs. 8 and 9. Data presented as mean ± standard error of the mean (SEM). Asterisks indicate a statistically significant difference at the indicated frequency (ANOVA, $p<0.01$).

Table 1

Antibody Characterization

Antibody	Immunogen	Species	Catolog No Lot No	Supplier	Dilution
Class III β-Tubulin	Antibody raised against microtubules derived from rat brain	Rabbit	MRB435p	Covance	1:200
CNPase	Antibody raised against human brain 2' 3'- cyclic nucleotide 3' phosphodiesterase	Mouse	MAB326 22040768	Chemicon	1:150
Connexin 29	Synthetic peptide representing amino acids 171–258 from C-terminus of mouse Connexin 29	Rabbit	sc-68377	Santa Cruz	1:200
Myosin VII-a	Amino acids 880–1077 from the tail reqion of Human Myosin-VIIa	Rabbit	25–6790 91103980	Proteus Bioscience	1:150
Na K- ATPase	Antibody raised against bovine cortex Na K-ATPase	Rabbit	31b	Dr George Siegel U M Med Sch, MI	1:2000
Neurofilament 200	Reacts to 200kD neurofilament in rat spinal cord extract	Mouse	N0142 073K4834	Sigma	1:200
Peripherin	Electrophoretically pure trp-E-peripherin fusion protein	Mouse	AB1530	Chemicon	1:150
Peripherin	Electrophoretically pure trp-E-peripherin fusion protein	Rabbit	AB1527	Chemicon	1:200